

Illumination strategies for space-bandwidth-time product improvement in Fourier ptychography

Haibo Xu¹, Cheng Li¹, Mingzhe Wei¹, Ziwen Zhou¹, and Longqian Huang^{*†1,2}

¹Institute of Laser Biomedicine, Zhejiang University, Hangzhou 310027, China

²School of Brain Science and Brain Medicine, Zhejiang University, Hangzhou 310058, China

Abstract

Fourier ptychography (FP) is a promising technique for high-throughput imaging. Reconstruction algorithms and illumination paradigm are two key aspects of FP. In this review, we mainly focus on illumination strategies in FP. We derive the space-bandwidth-time product (SBP-T) for the characterization of FP performance. Based on the analysis of SBP-T, we categorize the illumination strategy in FP effectively and discuss each category in detail.

Keywords— Fourier ptychography, space-bandwidth-time product, illumination

1 Introduction

Resolution and imaging field-of-view (FOV) are two factors that are mostly considered in imaging systems, especially in microscopy. Researchers have to choose microscopes with appropriate resolution and FOV for specific applications since there is a trade-off between them: high-resolution systems tend to have small FOV, and vice versa. Fourier ptychography (FP) is a synthetic approach that presumes high-throughput and high-resolution imaging by using more information through multiple captures. It captures multiple low-resolution, large FOV images and computationally combines them in the Fourier domain into a high-resolution, large FOV result [1].

The first demonstration of FP was made in 2013 by Zheng *et al.* [2]. With a programmable LED matrix, they proposed an iterative phase-retrieval-like ptychography algorithm in the Fourier domain and achieved a half-pitch resolution of 0.78 mm, a FOV of $\sim 120 \text{ mm}^2$ and a resolution-invariant depth of focus of 0.3 mm. Since then, FP has been developed in various directions, including higher resolution [3–7], faster imaging speed [8–20], and integration with other imaging modalities (X-ray [21], tomography [22, 23]). Although there are numerous ways to improve the FP technique, like changing optical configurations [4, 13], elaborating deep learning [10, 14, 20], we would like to consider the technique development from an illumination perspective.

In the history of FP development, researchers have made many efforts to modify illumination strategies, the ultimate goal of which is to improve imaging throughput (resolution, FOV) and speed. To categorize the illumination strategy fundamentally, we derive a universal and relatively fair metric for comparing different imaging techniques. This metric, termed space-frequency-time product (SBP-T [24]), combines space-frequency product (SBP [25]) which reflects the throughput of imaging and the acquisition time. With the theoretical analysis of SBP-T, we obtain the principle of designing the illumination strategy in FP, which includes increasing numerical aperture and decreasing low-resolution image acquisition times.

In the following sections, we investigate the illumination strategies for FP performance improvement. We first introduced the basic concept of FP, working principles, and processing pipelines in section 2; In section 3 we derive the comprehensive standard SBP-T for the judgment of the microscope’s performance. Based on the analysis of SBP-T, we demonstrated three categories of illumination strategies to improve it in section 4: (1) increase objective numerical aperture (subsection 4.2) (2) increase illumination numerical aperture (subsection 4.1); (3) reduce requisite sampling time (subsection 4.3). Finally, we summarize the paper and discuss the future development of FP in section 5.

*ALL authors contributed equally

†Corresponding Author: longqianh@zju.edu.cn

2 Principle of Fourier Ptychography

Fourier Ptychography (FP) is a technique that utilizes ptychography in the Fourier domain. It synthesizes multiple images taken at different spatial frequencies. By post-processing the obtained set of images, an image with a large FOV and high resolution is obtained. Here we briefly introduce the basic architecture and processing principle of FP.

2.1 Forward imaging model

The optical setup is shown in [Figure 1](#). The image sensor and sample are conjugated by a tube lens and an objective. Below the sample is the LED array that will be lit in sequence to provide spatial-frequency-varied illumination.

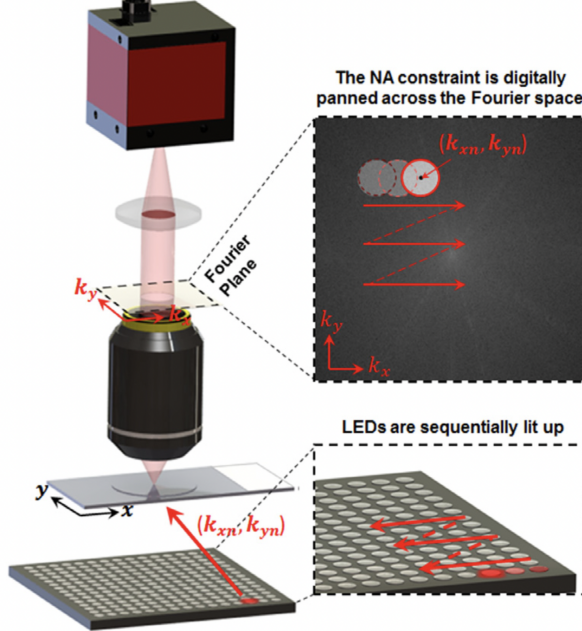


Figure 1: Optical setup of Fourier ptychography. Adapted from Ref. [26].

Assume the sample has the complex amplitude $A(r)$, $r = (x, y)$. When illuminated with the m^{th} LED light that has spatial frequency $k_m = (k_{xm}, k_{ym})$, the input amplitude to the imaging system is $E_{obj}(r)e^{ik_m \cdot r}$. The output optical field at the camera plane is

$$E(r) = p(r) * E_{obj}(r)e^{ik_m \cdot r}, \quad (1)$$

where p is the system (coherent) point spread function, and $*$ denotes convolution.

In the Fourier domain, the field is

$$\begin{aligned} \hat{E}(k) &= P(k) \cdot \hat{E}_{obj}(k - k_m), \\ I(r) &= \left| \mathcal{F}^{-1} [\hat{E}(k)] \right|^2, \end{aligned} \quad (2)$$

where \hat{E}_{obj} is the output at the objective focal plane, P is the pupil function (or coherent transfer function) of the microscope.

2.2 Recovery process

The processing of FP is an image synthesis procedure that iteratively completes the spatial frequency components. It uses captured low-resolution images I_{lm} to synthesize a high-resolution image I_h [2], where $m \in \{1, 2, \dots, N\}$ indicates the image is related to LED light that has the incident angle with spatial frequency $k_m = (k_{xm}, k_{ym})$.

2.2.1 Optimization model

The recovery can be formulated as the following optimization problem:

$$\min_{\hat{E}_{obj}(\mathbf{k}), P(\mathbf{k})} \sum_{m=1}^N \left\| I_m(\mathbf{r}) - \left| \mathcal{F} \left[P(\mathbf{k}) \cdot \hat{E}_{obj}(\mathbf{k} - \mathbf{k}_m) \right] \right|^2 \right\|_2. \quad (3)$$

To solve the above optimization problem, an iterative phase-retrieval-like algorithm is used. Assume the reconstructed high-resolution image I_h is the intensity of electrical field $E_h = \sqrt{I_h} e^{i\varphi_h}$. Firstly, an initial guess is made by setting $\varphi_h = 0$ and $I_h^{(0)} = \text{Up}(I_{l0})$, where Up denotes upsampling. Once the initial guess is done, an alternative projection iteration process starts:

1. Take Fourier transform of the last updated electrical field $E_h^{(n)}$: $\hat{E}_h^{(n)} = \mathcal{F} \left(E_h^{(n-1)} \right)$
2. Perform the selective spatial frequency pupil filtering: select the right pupil position in the spatial frequency domain, which is moved from the origin to $\mathbf{k}_m = (k_{xm}, x_{ym})$ by the angled incident light. We get $\psi^{(n)}(\mathbf{k}) = P(\mathbf{k}) \cdot \hat{E}_h^{(n)}(\mathbf{k} - \mathbf{k}_m)$. (Since the pupil function is the size of the low-resolution image, and E_h is the size of the high-resolution image, E_h needs to move its center to match P . For a brief, we just use $P \cdot \hat{E}_h$ in the following derivation)
3. Fourier transform back to the image plane: $E_h'^{(n)} = \mathcal{F}^{-1} \left(\psi^{(n)} \right) := \sqrt{I'_h} e^{i\varphi_h'^{(n)}}$, where P indicates the pupil function.
4. Utilize the angled light image constraint: replace the amplitude within the pupil region of $E_h'^{(n)}$ with the captured low-resolution image I_{lm} . We get $E_h^{(n+1)} = \sqrt{I_{lm}} e^{i\varphi_h'^{(n)}}$.

In one loop, all \mathbf{k}_m of the captured image sequence are used. It can be run repeatedly to get better results, and usually several is enough. Since the recovery process is adapted from the phase retrieval algorithm, the sample phase can be reconstructed, and therefore FP has the ability of quantitative phase imaging [26].

2.2.2 Aberration correction scheme

The ideal recovery process assumes no aberration, which means pupil function $P(\mathbf{k})$ in [Equation 3](#) is ignored. But in experiments, aberrations such as astigmatism and defocus often appear, and it is necessary to correct them. Therefore, aberration correction sometimes becomes an inevitable step in the recovery process.

In the FP literature, there are two correction schemes [27]: (1) adaptive pupil compensation and (2) joint high-resolution and pupil recovery. Both schemes require an appropriate estimation of the pupil function P . For example, in the defocus correction, P will add a phase term $\exp(i k_z z)$ to denote that the focal plane of the objective deviates the sample plane by a distance z .

Adaptive pupil compensation In the adaptive scheme, pupil estimation follows a closed-loop iteration as adaptive optics [27]. It searches pupil function (typically the defocus depth z) that minimizes the reconstruct metrics (usually the data fidelity measurement of $\|\sqrt{I_{hm}} - \sqrt{I_{lm}}\|$, where I_{hm} is the low-resolution image from the reconstructed high-resolution image that relates to \mathbf{k}_m LED light).

In Ref. [28], the algorithm aims at optimizing the term $\sum_r |\sqrt{I_{hm}} - \sqrt{I_{lm}}|$. To do this, it adds a correction factor c_m [28]:

$$c_m = \frac{\sum_r I_{hm}}{\sum_r I_{lm}}, \quad (4)$$

and change step 4 replacement in the recovery procedure to $E_h = \sqrt{c_m I_{lm}} e^{i\varphi_h'}$. This formula can be considered a weighted update where good reconstruction fidelity of each spatial frequency image takes the higher weight.

Joint pupil recovery In the joint scheme, pupil estimation and high-resolution object recovery are performed simultaneously in the iteration right after step 4.

The additional update rule is the following [29]:

$$\begin{aligned} E_h^{(n+1)} &= E_h^{(n)} + \alpha \cdot (I_{hm} - I_{lm}) \frac{P^{\dagger(n)}}{\max(|P^{(n)}|^2)}, \\ P^{(n+1)} &= P^{(n)} + \beta \cdot (I_{hm} - I_{lm}) \frac{E_h^{\dagger(n+1)}}{\max(|E_h^{(n+1)}|^2)}. \end{aligned} \quad (5)$$

Here \dagger is the conjugation operator, α, β are the step size of the update (can be set to 1). The update can be seen as compensation for the underestimated pupil [30].

3 Space-bandwidth-time product

Space-bandwidth product (SBP) is a critical characteristic in optical systems [25, 31]. It is defined by the range of location and spatial frequencies within which the signal is nonzero.

Formally, we denote the numerical aperture of the optical as NA, which consists of the objective numerical aperture and NA_o and illumination numerical aperture NA_i :

$$NA = NA_o + NA_i, \quad (6)$$

and the system resolution R can be computed as

$$R = \frac{\lambda}{2NA}. \quad (7)$$

Next, we denote the objective lens field-of-view as FOV, which is proportional to the spatial location range. Note that the cutoff spatial frequency is $\nu = 1/R$, then SBP can be computed as [32]:

$$\begin{aligned} SBP \sim FOV \cdot \nu^2 &= \frac{FOV}{R^2} \\ &= \frac{\lambda^2 \cdot FOV}{4NA^2}. \end{aligned} \quad (8)$$

The equation of SBP shows its relationship with FOV and NA. It is worth mentioning that there is a non-linear relation between FOV and NA. In general, with a high-NA objective lens, there will be a relatively small SBP because the FOV of an objective lens does not increase at the same pace as that of its NA [31].

Image acquisition speed is also essential in many biological applications. Therefore, the space-bandwidth-time product (SBP-T) is considered a more comprehensive standard in microscopy performance comparison [24]. It is defined as the SBP divided by its acquisition time T .

To derive SBP-T, we assume the mean processing time per pixel is Δt (including exposure and signal transmission), and the effective total pixels in one capture are estimated as $P = FOV/R$. Note that the system performance will decrease if the actual camera pixel P_{cam} is less than P , which can be avoided by changing to a better camera. Let the single-pixel computation time be Δt , and the necessary number of captures be N . The image acquisition time is

$$T = NP\Delta t = N \frac{FOV}{R} \Delta t. \quad (9)$$

Therefore, the expression of SBP-T is

$$\begin{aligned} SBP-T &= \frac{SBP}{T} = \frac{1}{NR\Delta t} \\ &= \frac{2NA}{N\lambda\Delta t} \\ &= \frac{2(NA_o + NA_i)}{N\lambda\Delta t}. \end{aligned} \quad (10)$$

Furthermore, if we assume a common FP illumination strategy (i.e., the LED array will be lit one by one), the required acquisition times N can be computed as (Figure 2)

$$\begin{aligned} NA_i &= n \sin \theta_2 = \frac{nh}{\sqrt{D^2 + h^2}} \implies D = \frac{NA_i h}{\sqrt{n^2 - NA_i^2}}, \\ N &= \left(\frac{2D}{\Delta d} \right)^2 = \frac{4h^2}{\Delta d^2 [(n/NA_i)^2 - 1]}, \end{aligned} \quad (11)$$

where h is the fixed distance between the sample and the LED array, and D is the half length of the LED array, corresponding to the maximum illumination NA. Δd is the LED pitch, and n is the refractive index between the LED and sample (illustrated in Figure 2).

Therefore, the final expression of SBP-T in common LED illumination is

$$SBP-T = \frac{\Delta d^2 (NA_o + NA_i) [(n/NA_i)^2 - 1]}{2h^2 \lambda \Delta t}. \quad (12)$$

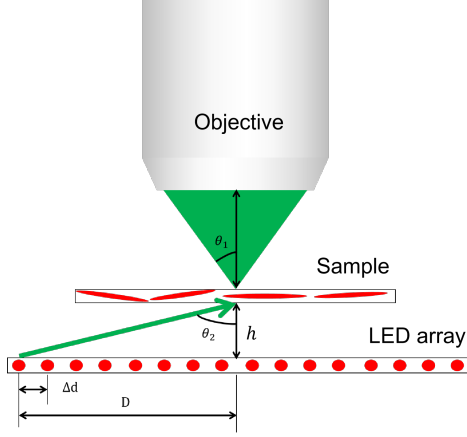


Figure 2: One-dimensional illustration of estimating required acquisition time.

4 Illumination strategies for SBP-T improvement

We have derived SBP-T for common LED illumination FP (Equation 12). For analysis, Equation 10 gives us theoretical directions for improving FP. To be more specific, we set the goal as maximizing SBP-T, and one can achieve this by three means: increasing NA_o , increasing NA_i , or decreasing required acquisition time N . Besides, we do not discuss shortening the exposure and pixel transferring time Δt here, which can also improve SBP-T but is straightforward by increasing light transport efficiency.

4.1 Increasing illumination NA

There are three approaches proposed to increasing NA_i : (1) immersing in the high refractive-index medium; (2) using a large-angle illumination condenser; (3) using a reflection-mode configuration.

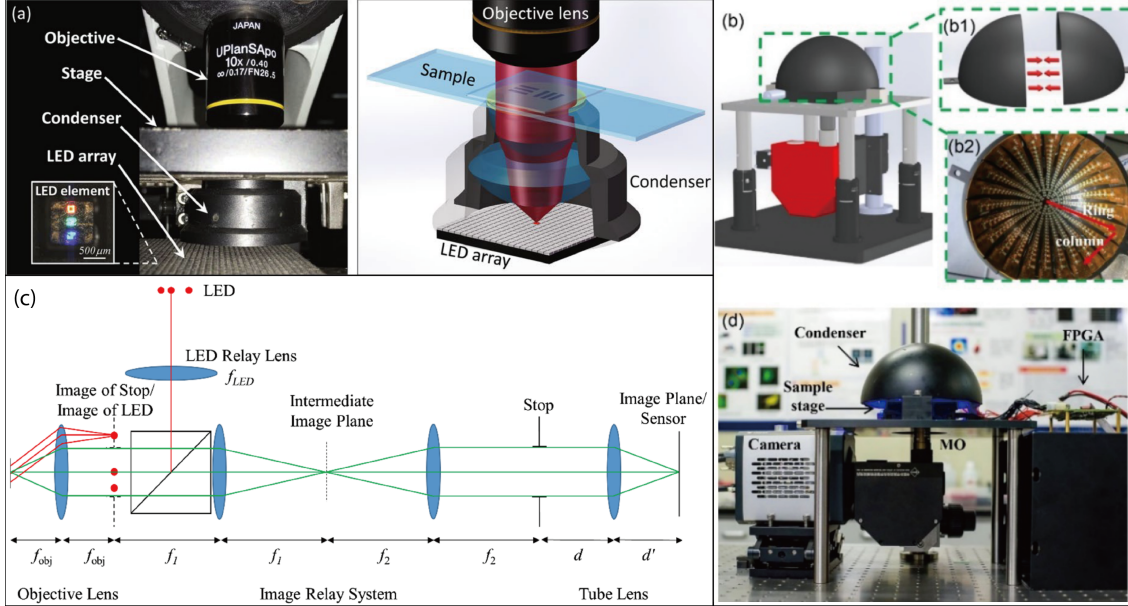


Figure 3: Three approaches for illumination NA improvement. (a) immersing condenser in oil [5]. (b,d) using hemisphere condenser lens [6]. (c) reflective FP setup [4].

As shown in Figure 3 (a), Sun *et al.* straightforwardly designed an oil-immersion condenser LED array to improve NA_i [5]. The high refractive-index oil enables the condenser to produce higher spatial frequency incident light, which

endows them to achieve a final effective NA equal to 1.6, with a 10x, 0.4NA objective lens. In Figure 3 (b,d), Pan *et al.* designed a hemisphere digital condenser to provide high-angle programmable plane-wave illuminations of 0.95NA and realized a subwavelength resolution (a half-pitch resolution of 244 nm with the incident wavelength of 465 nm across a wide FOV of 14.60 mm²).

Pacheco *et al.* demonstrated a reflective FP architecture in Ref. [4], and the optical setup is shown in Figure 3 (c). By placing the LED at the back focal plane of the objective and setting the position of the LED to be greater than the radius of the objective's entrance pupil, the illumination NA will be equal to the objective NA, hence the maximum synthesized NA is $2N_{\text{A}_o}$. Furthermore, by placing the imaging stop outside the illumination path in the reflective FP, the NA of the illumination can be much greater than the NA of the imaging system. They experimentally demonstrated a synthesized NA increased by a factor of 4.5 using the proposed optical concept.

4.2 Increasing objective NA

Frequency mixing between the object and the illumination allows the recovery of object frequencies beyond the diffraction-limited detection bandpass. by using nonzero-spatial-frequency illumination, the high frequency of the object beyond the detection bandpass of the objective lens is encoded (or moved) into a lower frequency and hence can be captured. This is equivalent to the increase of effective objective NA. As demonstrated in blind structured illumination microscopy [33], using various speckle illumination, it is possible to obtain better resolution (larger $N_{\text{A}_{\text{eff}}}$) without knowing the exact illumination pattern. This illumination strategy is also transplanted in FP architecture, which we term as *speckle illumination*.

When speckle illumination was first proposed in FP [34], it substituted the traditional LED array with a laser and diffuser. The semitransparent diffuser was placed before the sample, and the sample was translated to obtain various speckle patterns (Figure 4 (b)). This setup was modified by making the diffuser the moving part [35] (Figure 4 (a)). In Ref. [36], Song *et al.* placed the diffuser behind the sample (Figure 4 (c)). Benefiting from the novel setup, the sample thickness becomes irrelevant, and they can focus on the wavefront that exits the sample. They showed a 4.5-fold resolution gain over the diffraction limit.

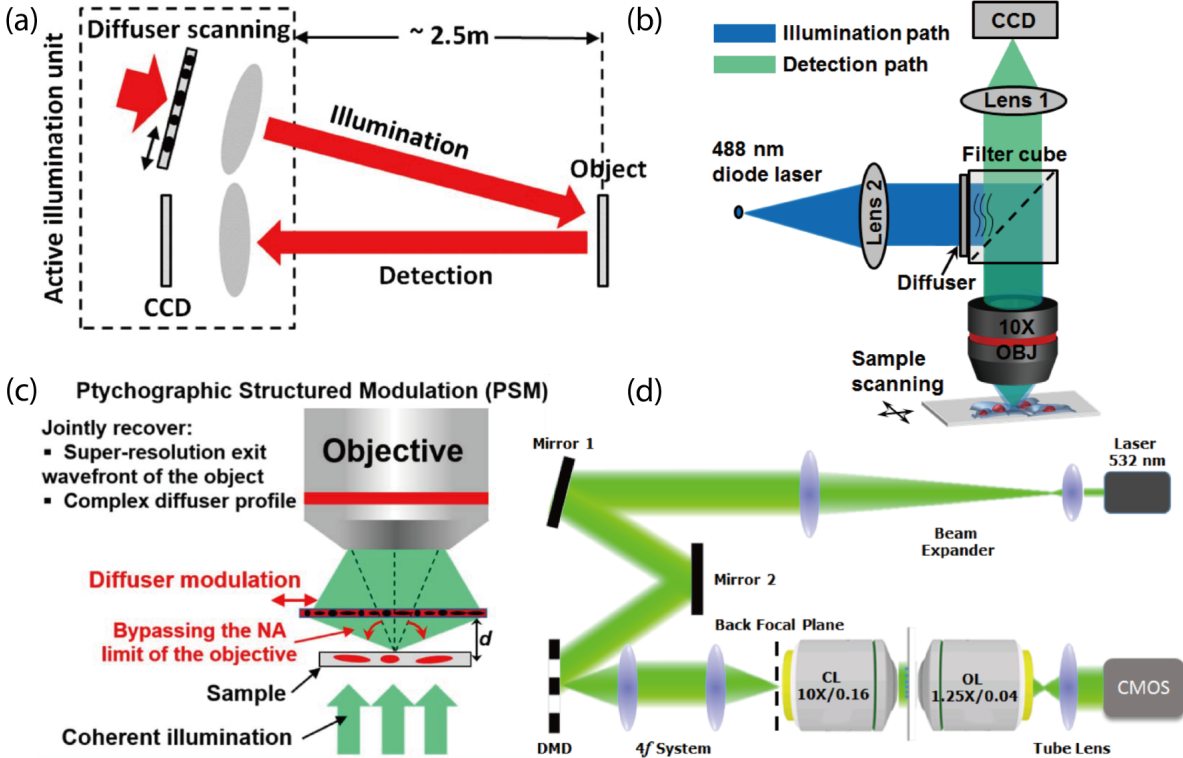


Figure 4: Speckle illumination methods for $N_{\text{A}_{\text{eff}}}$ improvement. (a) speckle illumination via diffuser scanning [35]. (b) speckle illumination via sample scanning. (c) speckle illumination with a diffuser placed behind the sample [36]. (c) speckle illumination using a digital micromirror device (DMD) [9].

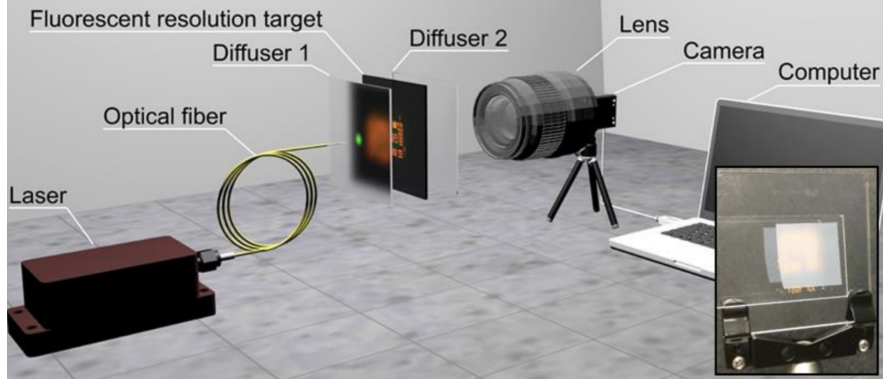


Figure 5: The system setup of the reported double diffuser strategy for speckle illumination FP. Adapted from Ref. [37].

In 2018, Kaikai Guo *et al.* further developed the diffuser speckle illumination method [37]. They obtained 13 times resolution enhancement by sandwiching the sample between two diffusers (Figure 5). By tilting the input wavefront, they raster scan the unknown speckle pattern and capture the corresponding low-resolution image that passes through the turbidity layer. The front-behind diffusers, together with the joint object-speckle-PSF reconstruction algorithm allow them to grasp higher object frequency that is otherwise untouchable.

A new approach for speckle generating is proposed by elaborating on the digital micromirror device (DMD) [9]. Figure 4 (d) shows the configuration of the DMD-based laser-illumination FPM system. The use of DMD can significantly accelerate the illumination pattern generation speed and get rid of the irritating procedure of moving the sample or diffuser.

The reconstruction process is similar to the original FP recovery, where the pupil function becomes the unknown speckle pattern, and joint pupil recovery (section 2.2.2) for speckle pattern guessing is always employed. Figure 6 gives a direct overview of reconstruction algorithms in speckle-illumination FP.

	Coherent FP	Incoherent FP
Step 1	$I_{obj}e^{i\phi}$	I_{obj}
Step 2	$I_{tn}=I_{obj}e^{i\phi} \cdot Ae^{ikx}$	$I_{tn}=I_{obj} \cdot P_n$
Step 3	Update the image in the Fourier domain	
Step 4	Update the image in the spatial domain	
Step 5	Repeat for other illumination angles	Repeat for other illumination patterns
Step 6	Repeat steps 2 - 5 until solution converges	

Figure 6: Comparison of LED-array illumination FP and speckle illumination FP. Adapted from Ref. [35].

As an extension of speckle illumination FP, a method called near-field Fourier ptychography was proposed for photography beyond microscopy. This is realized by placing the object at a short defocus distance with a large Fresnel number, and a speckle pattern with fine spatial features is cast on the object. The difference between near-field FP and original speckle illumination FP is the propagation of diffused light. A diffraction propagation equation has to be inserted into the reconstruction process.

4.3 Acquisition time reduction

4.3.1 Sparse illumination

To address the efficiency problem in current FPM, some researchers investigated the spatial spectrum redundancy of natural images in the Fourier domain and proposed sampling strategies to decrease the requisite illumination angles during acquisition and correspondingly decrease the shutter count N of the FP technique.

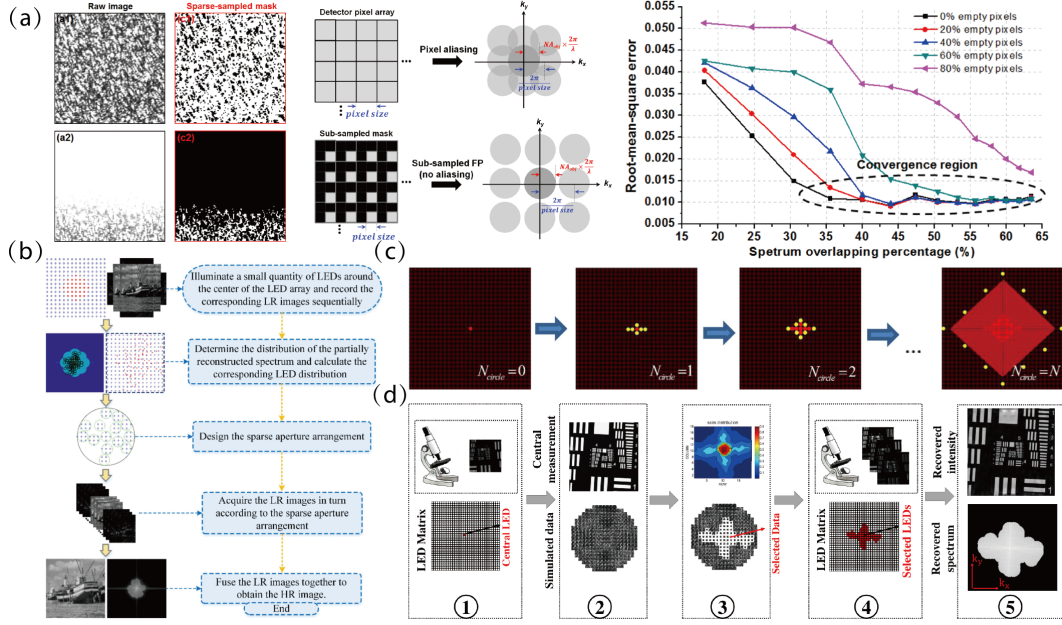


Figure 7: Sparse illumination for FP acquisition reduction. (a) spatial sparse sampling via masks, spectral sparse sampling via subsampled pixels, spatial-spectral redundancy curve [8]. (b) Spectral-distribution-based illumination LED selection [38]. (c) Rhombus-shaped LED array illumination [39]. (d) SSIM-based spectral selection scheme [40].

In 2014, Dong *et al.* investigated the spectral-spatial data redundancy requirement in FP, which is the theoretical basis of the sparse illumination strategy [8]. They experimentally examined how much spectrum overlapping (in the spectral domain) and how many pixels need to update is needed (in the spatial domain) for a decent FP reconstruction. Finally, they proposed a sparse update using a mask in the spatial domain (which essentially drops the over-exposure and under-exposure pixels) and a sub-sampled detector pixel array. By using the proposed sparse sampling framework, they shorten the acquisition time of the FP by $\sim 50\%$.

To achieve sparse sampling, Bian [41] proposed a highly efficient method termed adaptive Fourier ptychography (AFP) in 2014. It applies content-adaptive illumination for FP to capture the most informative parts of the scene's spatial spectrum. By selectively illuminating circle by circle towards the high-frequency direction, it reduces acquisition time by around 30%–60%. In 2015, Zhang [40] proposed a self-learning-based method, which utilizes the single captured central-illumination measurement and simulates the angled illumination. Based on the structural similarity metric (SSIM) between the simulated image spectrum and the measurement spectrum, they can select images used in the FPM reconstruction. The number of acquired images can be reduced from 225 to 70, with a time reduction of $\sim 70\%$. The flowchart of the method is shown in Figure 7 (d). Similarly, Cheng [38] proposed a sparse illumination method based on maximum object spectral information. The flow chart of their proposed method is shown in Figure 7 (b). Based on the relationship between the spectrum distribution of the specimen and the LED array sampling pattern, they analyze the spectrum of captured center-illumination low-resolution image to manually select the informative position and design a sparse aperture arrangement accordingly. The total number of LEDs sampled is reduced by 40% to 55% and the total processing time for the sampling is reduced from 304.31 s to 124.86 s compared with the traditional FPM sampling method.

Great development in deep learning also allows researchers to design illumination patterns intelligently. In 2019, Cheng [15] used a deep neural network to achieve single-shot imaging, reducing the acquisition time in Fourier ptychographic microscopy by a factor of 69. They proposed an illumination pattern co-optimization framework. In the training phase, shown in Figure 8 (a), they use deep learning to find a single LED illumination pattern, where

the LED pattern corresponds to a neural network layer. In the evaluation phase (shown in Figure 8 (b)), they first program the LED matrix with a static pattern. Then, for each sample, they take a single image and process it through the trained neural network layers to get the high-resolution complex object.

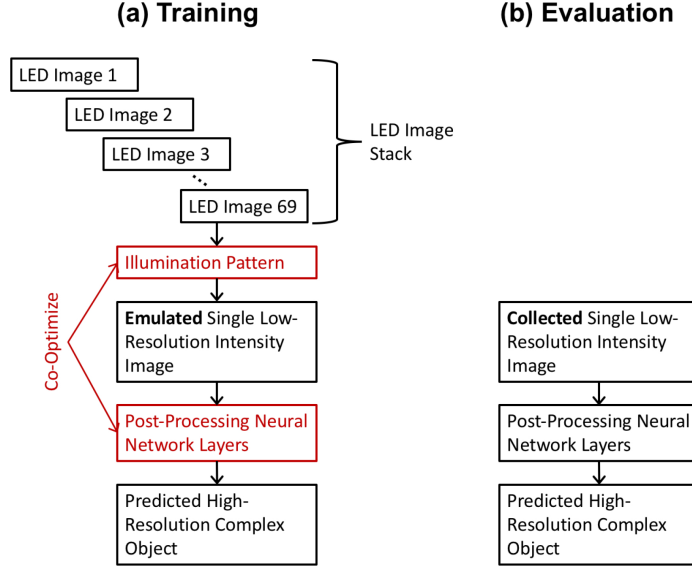


Figure 8: Overview of the training and evaluation steps in optimization. Adapted from Ref. [15]

As a kind of sparse illumination, Mao [39] proposed a method based on the rhombus-shaped LED array. They selected the most important LEDs as the rhombus circle expanded. Compared to the reconstruction process under conventional illumination, it is reduced the total time from 99.126 s to 25.396 s, with a reduction of $\sim 77\%$. The selected N LEDs by following the shape of the rhombus are shown in Figure 7 (c).

4.3.2 Multiplexing

Multiplexing is also an effective acceleration approach in FP imaging. In 2014, Tian *et al.* proposed an angle-multiplexing illumination (also called source-coded illumination [42]), where multiple randomly selected LEDs are used to illuminate each image [43]. For example, illumination patterns designed according to random codes and resulting images are shown in Figure 9 (a). With an appropriate reconstruction algorithm, this scheme allows them to fill the Fourier space faster, which can greatly reduce the sampling time and data size in FP. They demonstrated the large SBP-T advantages of angle-multiplexing illumination (46 megapixels/s) with improved initialization strategy and reconstruction algorithm in Ref. [42].

In contrast to angle-multiplexing for faster filling in the Fourier domain, another multiplexing strategy is wavelength multiplexing. The proposed wavelength multiplexing approach in Ref. [11] can speed up the acquisition process of FP several folds. Figure 9 (c) illustrates the concept of multicolor LEDs lighting up simultaneously to illuminate different circular regions in a sample's Fourier plane. In this way, different wavelengths are used to label the different spatial frequencies of the samples, which can be decoded via the corresponding algorithms. In experiments, they demonstrated an RGB multiplexed illumination and used an RGB camera for channel de-multiplexing (Figure 9 (b)). They also proposed an accelerated detection approach by hardware de-multiplexing, using a grating and camera array, as shown in Figure 9 (d).

Reconstruction algorithms for de-multiplexing is essential to multiplexing methods. Several algorithms based on the multiplexing principle have been proposed simultaneously as the multiplexing strategy is proposed [11, 42, 44]. Algorithm robustness [45] and acceleration [46] have also been investigated. Since the reconstruction algorithm is the post-processing step in FP and has little contribution in improving SBP-T (note that Δt in Equation 10 is only related to exposure and data transfer time when capturing), we would not give a detailed discussion here.

5 Summary

In this paper, we reviewed illumination strategies for improving SBP-T in FP. Based on the analysis of SBP-T, we choose to investigate FP illumination methods from the aspect of NA improvement and necessary image acquisition

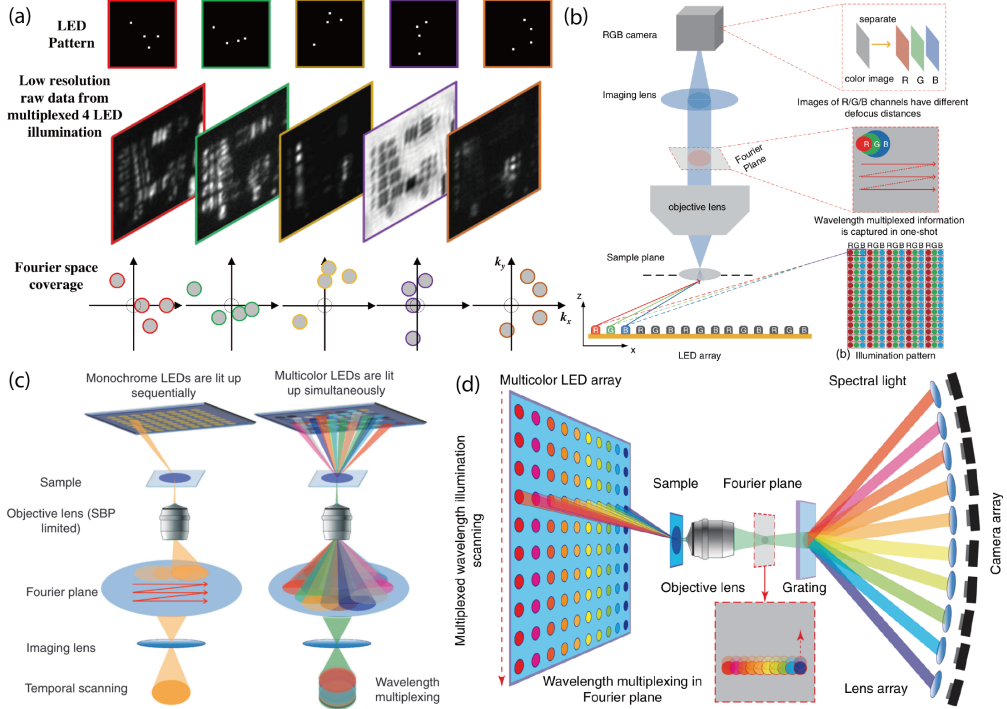


Figure 9: Multiplexed illumination. (a) Angle-multiplexing [43]. (b) RGB wavelength-multiplexing demonstrated in Ref. [11]. (c) Concept of wavelength multiplexing with multicolor LEDs [11]. (d) Concept of wavelength multiplexing with grating and camera array for accelerated detection [11].

reduction: (i) For NA improvement, we first discussed methods regarding illumination NA: the utilization of a specially designed condenser lens and a reflective optical setup. Then we compared different speckle illumination configurations for improving objective NA. The speckle illumination in FP borrows the concept of blind-SIM and shows good results in improving the synthetic NA. It is worth mentioning that it endows FP with the ability of fluorescence imaging, as the intensity-varied speckle can encode fluorescence emitting while angle-varied LED illumination cannot. (ii) For image acquisition reduction, we discussed sparse illumination and multiplexed illumination. Both methods demonstrate the ability to reduce the capturing times. There is also a method called state-multiplexing, which uses multiple light sources to illuminate simultaneously the incoherent superposition of the transmission profiles with different coherent states [44]. Since this multiplexing method cannot reduce the acquisition time N effectively, we do not put it in the multiplexing illumination class.

In addition, we think it is necessary to calculate the SBP-T of each proposed FP method and compare them quantitatively, but we cannot complete that here due to time and device limitations (here we give a brief comparison table with a limited number of methods).

Table 1: FP technique comparison without SBP-T.

Reference	Full-pitch Resolution [47]	FOV	Speed
<i>Opt. Express</i> 30 , 29189 (2022).	0.3 um	0.65mm × 0.65mm	3s
<i>Opt. Express</i> 27 , 644–656 (2019).	<2 um	/	1.14s
<i>Opt. Express</i> , 26 , 23119–23131 (2018).	0.488 um	14.6 mm ²	4.15s
<i>Sci Rep</i> 7 , 1187 (2017).	308 um	2.34 mm ²	/
<i>J. Biomed. Opt</i> 22 , 066006 (2017).	1.56 um	/	~ 100s
<i>Optica</i> , 2 , 904–911 (2015).	<2 um	/	0.8s
<i>Opt. Express</i> 22 , 20856 (2014).	0.66 um	15 um × 15 um	/
<i>Nature Photon</i> 7 , 739–745 (2013).	1.56 um, axial 0.3 mm	120 mm ²	3min

Furthermore, we would like to mention the illumination strategy of FP can be designed specifically for different

applications. For instance, because the reconstruction algorithm of FP is phase-retrieval-like, it can recover the phase information with good quality. This ability enables FP to be applied in quantitative phase imaging (QPI), and corresponding illumination strategies can be specifically modified. In 2018, a reduced ring illumination was proposed by Sun *et al.* [17] to reduce the acquisition time in QPI greatly. They analyzed the quantitative phase imaging process in FP and tuned the FP illumination pattern for phase imaging applications. They demonstrated that low-frequency phase components could be completely covered at annular illumination when coherent parameter $S = \text{NA}_i/\text{NA}_o = 1$. A video-rate FP based on annular illuminations named AIFPM is reported, which uses an annular illumination scheme by only lighting up LED elements located on a ring with the illumination NA matching the NA_o . AIFPM reduces the exposure time for each image to only 10 ms, thus the total data acquisition time is 0.12 s for 12-LED scanning and can be reduced to 0.04 s if the fastest 4-LED scanning mode is used. The results show an SBP-T of 411 megapixels/s for in-vitro Hela cell mitosis and apoptosis at a frame rate 25Hz. Multiplexing has been applied in QPI applications. A single-shot QPI method based on color-multiplexed FPM was proposed by Sun *et al.* [12], where three monochromatic intensity images are sufficient to achieve high-accuracy phase retrieval by combining phase deconvolution and FPM iterative refinement.

For future development of FP, we think reflective FP is a significant direction for in-vivo applications. Researchers have demonstrated it [4] high illumination NA property, and more improvements are expected. In addition, combining different illumination strategies is also promising. Since speckle illumination has shown a fluorescence imaging ability [34], it can be combined with reflective configuration hopefully. Sparse illumination and wavelength multiplexing can also be combined to boost image-capturing speed [11]. Finally, novel optical setups that extend the FP scheme is also expected. For example, a concept of single-shot FP, with a different optical setup is proposed [13], encouraging us of the great potential of FP future development.

Acknowledgments We thank Prof. Dawei Di, Prof. Pan Wang, and Prof. Ke Si for their generous teaching in academic writing.

Conflict of interest The authors declare no conflicts of interest related to this article.

References

- [1] Pavan Chandra Konda, Lars Loetgering, Kevin C Zhou, Shiqi Xu, Andrew R Harvey, and Roarke Horstmeyer. Fourier ptychography: current applications and future promises. *Optics express*, 28(7):9603–9630, 2020.
- [2] Guoan Zheng, Roarke Horstmeyer, and Changhuei Yang. Wide-field, high-resolution fourier ptychographic microscopy. *Nature photonics*, 7(9):739–745, 2013.
- [3] Xiaoze Ou, Roarke Horstmeyer, Guoan Zheng, and Changhuei Yang. High numerical aperture fourier ptychography: principle, implementation and characterization. *Optics express*, 23(3):3472–3491, 2015.
- [4] Shaun Pacheco, Guoan Zheng, and Rongguang Liang. Reflective fourier ptychography. *Journal of biomedical optics*, 21(2):026010, 2016.
- [5] Jiasong Sun, Chao Zuo, Liang Zhang, and Qian Chen. Resolution-enhanced fourier ptychographic microscopy based on high-numerical-aperture illuminations. *Scientific reports*, 7(1):1–11, 2017.
- [6] An Pan, Yan Zhang, Kai Wen, Meiling Zhou, Junwei Min, Ming Lei, and Baoli Yao. Subwavelength resolution fourier ptychography with hemispherical digital condensers. *Optics Express*, 26(18):23119–23131, 2018.
- [7] He Zhang, Shaowei Jiang, Jun Liao, Junjing Deng, Jian Liu, Yongbing Zhang, and Guoan Zheng. Near-field fourier ptychography: super-resolution phase retrieval via speckle illumination. *Optics express*, 27(5):7498–7512, 2019.
- [8] Siyuan Dong, Zichao Bian, Radhika Shiradkar, and Guoan Zheng. Sparsely sampled fourier ptychography. *Optics express*, 22(5):5455–5464, 2014.
- [9] Cuifang Kuang, Ye Ma, Renjie Zhou, Justin Lee, George Barbastathis, Ramachandra R Dasari, Zahid Yaqoob, and Peter TC So. Digital micromirror device-based laser-illumination fourier ptychographic microscopy. *Optics express*, 23(21):26999–27010, 2015.
- [10] Armin Kappeler, Sushobhan Ghosh, Jason Holloway, Oliver Cossairt, and Aggelos Katsaggelos. Ptychnet: Cnn based fourier ptychography. In *2017 IEEE International Conference on Image Processing (ICIP)*, pages 1712–1716. IEEE, 2017.
- [11] You Zhou, Jiamin Wu, Zichao Bian, Jinli Suo, Guoan Zheng, and Qionghai Dai. Fourier ptychographic microscopy using wavelength multiplexing. *Journal of biomedical optics*, 22(6):066006, 2017.

- [12] Jiasong Sun, Qian Chen, Jialin Zhang, Yao Fan, and Chao Zuo. Single-shot quantitative phase microscopy based on color-multiplexed fourier ptychography. *Optics letters*, 43(14):3365–3368, 2018.
- [13] Xiaoliang He, Cheng Liu, and Jianqiang Zhu. Single-shot aperture-scanning fourier ptychography. *Optics Express*, 26(22):28187–28196, 2018.
- [14] Thanh Nguyen, Yujia Xue, Yunzhe Li, Lei Tian, and George Nehmetallah. Deep learning approach for fourier ptychography microscopy. *Optics express*, 26(20):26470–26484, 2018.
- [15] Yi Fei Cheng, Megan Strachan, Zachary Weiss, Moniher Deb, Dawn Carone, and Vidya Ganapati. Illumination pattern design with deep learning for single-shot fourier ptychographic microscopy. *Optics express*, 27(2):644–656, 2019.
- [16] Jizhou Zhang, Tingfa Xu, Ziyi Shen, Yifan Qiao, and Yizhou Zhang. Fourier ptychographic microscopy reconstruction with multiscale deep residual network. *Optics Express*, 27(6):8612–8625, 2019.
- [17] Jiasong Sun, Chao Zuo, Jialin Zhang, Yao Fan, and Qian Chen. High-speed fourier ptychographic microscopy based on programmable annular illuminations. *Scientific reports*, 8(1):1–12, 2018.
- [18] Yi Xiao, Shiyuan Wei, Shaolong Xue, Cuifang Kuang, Anli Yang, Maoliang Wei, Hongtao Lin, and Renjie Zhou. High-speed fourier ptychographic microscopy for quantitative phase imaging. *Optics Letters*, 46(19):4785–4788, 2021.
- [19] Tomas Aidukas, Pavan C Konda, and Andrew R Harvey. High-speed multi-objective fourier ptychographic microscopy. *Optics Express*, 30(16):29189–29205, 2022.
- [20] Vittorio Bianco, Mattia Delli Priscoli, Daniele Pirone, Gennaro Zanfardino, Pasquale Memmolo, Francesco Bardozzo, Lisa Miccio, Gioele Ciaparrone, Pietro Ferraro, and Roberto Tagliaferri. Deep learning-based, misalignment resilient, real-time fourier ptychographic microscopy reconstruction of biological tissue slides. *IEEE Journal of Selected Topics in Quantum Electronics*, 28(4):1–10, 2022.
- [21] Jason Holloway, Yicheng Wu, Manoj K Sharma, Oliver Cossairt, and Ashok Veeraraghavan. Savi: Synthetic apertures for long-range, subdiffraction-limited visible imaging using fourier ptychography. *Science advances*, 3(4):e1602564, 2017.
- [22] Roarke Horstmeyer, Jaebum Chung, Xiaoze Ou, Guoan Zheng, and Changhuei Yang. Diffraction tomography with fourier ptychography. *Optica*, 3(8):827–835, 2016.
- [23] Chao Zuo, Jiasong Sun, Jiaji Li, Anand Asundi, and Qian Chen. Wide-field high-resolution 3d microscopy with fourier ptychographic diffraction tomography. *Optics and Lasers in Engineering*, 128:106003, 2020.
- [24] Daixuan Wu, Jiawei Luo, Guoqiang Huang, Yuanhua Feng, Xiaohua Feng, Runsen Zhang, Yuecheng Shen, and Zhaohui Li. Imaging biological tissue with high-throughput single-pixel compressive holography. *Nature Communications*, 12(1):1–12, 2021.
- [25] Adolf W. Lohmann, Rainer G. Dorsch, David Mendlovic, Carlos Ferreira, and Zeev Zalevsky. Space-bandwidth product of optical signals and systems. *Journal of the Optical Society of America A*, 13(3):470, March 1996.
- [26] Xiaoze Ou, Roarke Horstmeyer, Changhuei Yang, and Guoan Zheng. Quantitative phase imaging via fourier ptychographic microscopy. *Opt. Lett.*, 38(22):4845–4848, Nov 2013.
- [27] Guoan Zheng. *Fourier ptychographic imaging: a MATLAB tutorial*. Morgan & Claypool Publishers, 2016.
- [28] Zichao Bian, Siyuan Dong, and Guoan Zheng. Adaptive system correction for robust fourier ptychographic imaging. *Optics express*, 21(26):32400–32410, 2013.
- [29] Xiaoze Ou, Guoan Zheng, and Changhuei Yang. Embedded pupil function recovery for fourier ptychographic microscopy. *Opt. Express*, 22(5):4960–4972, Mar 2014.
- [30] Andrew M. Maiden and John M. Rodenburg. An improved ptychographical phase retrieval algorithm for diffractive imaging. *Ultramicroscopy*, pages 1256–1262, September 2009.
- [31] Jongchan Park, David J Brady, Guoan Zheng, Lei Tian, and Liang Gao. Review of bio-optical imaging systems with a high space-bandwidth product. *Advanced Photonics*, 3(4):044001, 2021.
- [32] An Pan, Chao Zuo, and Baoli Yao. High-resolution and large field-of-view fourier ptychographic microscopy and its applications in biomedicine. *Reports on Progress in Physics*, 83(9):096101, 2020.
- [33] E. Mudry, K. Belkebir, J. Girard, J. Savatier, E. Le Moal, C. Nicoletti, M. Allain, and A. Sentenac. Structured illumination microscopy using unknown speckle patterns. *Nature Photonics*, 6(5):312–315, 2012.
- [34] Siyuan Dong, Pariksheet Nanda, Radhika Shiradkar, Kaikai Guo, and Guoan Zheng. High-resolution fluorescence imaging via pattern-illuminated fourier ptychography. *Optics express*, 22(17):20856–20870, 2014.

- [35] Siyuan Dong, Pariksheet Nanda, Kaikai Guo, Jun Liao, and Guoan Zheng. Incoherent fourier ptychographic photography using structured light. *Photonics Research*, 3(1):19–23, 2015.
- [36] Pengming Song, Shaowei Jiang, He Zhang, Zichao Bian, Chengfei Guo, Kazunori Hoshino, and Guoan Zheng. Super-resolution microscopy via ptychographic structured modulation of a diffuser. *optics letters*, 44(15):3645–3648, 2019.
- [37] Kaikai Guo, Zibang Zhang, Shaowei Jiang, Jun Liao, Jingang Zhong, Yonina C. Eldar, and Guoan Zheng. 3-fold resolution gain through turbid layer via translated unknown speckle illumination. *Biomedical Optics Express*, 9(1):260–275, 2018.
- [38] Haobo Cheng, Xin Chen, Yongfu Wen, Huaying Wang, and Hui Li. Sparse aperture arrangement for periodic led array sampling in a fourier ptychography microscopy system. *Applied Optics*, 58(32):8791–8801, 2019.
- [39] Haifeng Mao, Xiaohui Wu, Jufeng Zhao, Guangmang Cui, and Jinxing Hu. An efficient fourier ptychographic microscopy method based on optimized pattern of led angle illumination. *Biomedical Optics Express*, 5:102920, 2020.
- [40] Yongbing Zhang, Weixin Jiang, Lei Tian, Laura Waller, and Qionghai Dai. Self-learning based fourier ptychographic microscopy. *Optics express*, 23(14):18471–18486, 2015.
- [41] Liheng Bian, Jinli Suo, Guohai Situ, Guoan Zheng, Feng Chen, and Qionghai Dai. Content adaptive illumination for fourier ptychography. *Optics letters*, 39(23):6648–6651, 2014.
- [42] Lei Tian, Ziji Liu, Li-Hao Yeh, Michael Chen, Jingshan Zhong, and Laura Waller. Computational illumination for high-speed in vitro Fourier ptychographic microscopy. *Optica*, 2(10):904–911, October 2015. Publisher: Optica Publishing Group.
- [43] Lei Tian, Xiao Li, Kannan Ramchandran, and Laura Waller. Multiplexed coded illumination for fourier ptychography with an led array microscope. *Biomedical optics express*, 5(7):2376–2389, 2014.
- [44] Siyuan Dong, Radhika Shiradkar, Pariksheet Nanda, and Guoan Zheng. Spectral multiplexing and coherent-state decomposition in fourier ptychographic imaging. *Biomedical optics express*, 5(6):1757–1767, 2014.
- [45] Li-Hao Yeh, Jonathan Dong, Jingshan Zhong, Lei Tian, Michael Chen, Gongguo Tang, Mahdi Soltanolkotabi, and Laura Waller. Experimental robustness of fourier ptychography phase retrieval algorithms. *Optics express*, 23(26):33214–33240, 2015.
- [46] Emrah Bostan, Mahdi Soltanolkotabi, David Ren, and Laura Waller. Accelerated wirtinger flow for multiplexed fourier ptychographic microscopy. In *2018 25th IEEE International Conference on Image Processing (ICIP)*, pages 3823–3827. IEEE, 2018.
- [47] Roarke Horstmeyer, Rainer Heintzmann, Gabriel Popescu, Laura Waller, and Changhuei Yang. Standardizing the resolution claims for coherent microscopy. *Nature Photonics*, 10(2):68–71, 2016.